Observations with fast visible cameras in high power Deuterium plasma experiments in the JET ITER-like wall tokamak

U. Losada, A. Manzanares, I. Balboa[b], S. Silburn[b], J. Karhunen[c], Pedro J. Carvalho[d], A. Huber[e], V. Huber[e], Emilia R. Solano, E. de la Cal, and JET contributors*

Laboratorio Nacional de Fusión - Ciemat , Madrid, Avda. Complutense, nº 40, 28040, Spain
[b] *Culham Centre for Fusion Energy, UKAEA, Culham, Oxford, United Kingdom*
[c]*Department of Applied Physics, Aalto University, P O Box 14100, FI-00076 Aalto, Finland*
[d] *Instituto de Plasmas e Fusão Nuclear, Instituto Superior Técnico, Universidade de Lisboa, Av. Rovisco Pais, 1049-001 Lisboa, Portugal*
[e] *Forschungszentrum Jülich GmbH, Institut für Energie- und Klimaforschung—Plasmaphysik, Partner of the Trilateral Euregio Cluster (TEC), 52425 Jülich, Germany*
* See the author list of "E. Joffrin et al. Nuclear fusion 59.11 (2019): 112021"
ulises.losada@ciemat.es

Abstract: High speed visible imaging allows to visualize the 2-dimensional dynamics of fast phenomena in the boundary layer of fusion plasmas. Here we describe the two high speed visible cameras currently operating in the JET tokamak, enabling the simultaneous observation of a large fraction of the JET tokamak vacuum vessel with the appropriate configuration for many different plasma phenomena. As an example we discuss recent observations on the spatial and temporal dynamics of visible emission at the outer wall during Edge Localized Modes (ELMs) and the penetration of Shattered Injected Pellet (SPI) into the plasma.

1. Introduction:

The Joint European Torus (JET) ($R = 2.96\ m,\ r = 1{,}25\ m$), operating with an all metallic wall (ITER-like wall (ILW)) [1, 2], is the largest tokamak currently in operation. High power Deuterium plasmas, (NBI up to 32 MW + 8 MW of ICRF power) were achieved during the last experimental campaign (called C38), in preparation for Deuterium-Tritium (D-T) plasmas.

More than 30 cameras and pyrometers are installed in the JET. These elements can be grouped in three main categories: First, four operational cameras which provide a real time wide-angle view of the JET vacuum vessel from different toroidal sectors. Second: A system of absolutely calibrated near infrared (IR) CCD cameras for active protection were installed in order to monitor the temperature of wall surfaces during plasma pulses [3]. This system combines wide-angle and divertor-view cameras [4, 5] which can interrupt the plasma pulse by a feedback system. Finally, scientific cameras: four Divertor and wide-angle view IR cameras for thermographic studies, two wide-angle view visible cameras for spectroscopy and two fast visible cameras, that will be described in the present work. The monitoring of visible and IR emission from different regions of the vacuum chamber will be also fundamental in ITER for protection and scientific purposes [6].

Fast framing cameras are non-perturbing diagnostics used to observe the 2-dimensional dynamics of fast phenomena in fusion plasmas [7-11]. A first fast visible camera, named as KL8A, was installed in JET [14] near the equatorial port and looking through an endoscope shared with an IR camera [15], providing a wide-angle view of the JET vacuum vessel from octant 8. It has demonstrated its usefulness to observe disruptions [16], pellets, ELMs [20] and the plasma breakdown. More recently, an additional fast visible camera, known as KLDT-E5WE, was installed outside the JET bio-shield in order to avoid radiation damage and allowing its operation during the next D-T campaign. The combination of both systems allows the observation of a large fraction of the vacuum vessel with the appropriate configuration for different plasma phenomena. In this article we describe the two fast visible cameras

installed at JET and we explain recent observations on ELMs and SPI pellets. The working principle of fast visible cameras in JET as well as its operation and analysis procedures are explained in the section 2. In section 3 are shown the observation of ELMs in the outer wall and the monitoring of SPI pellet penetration, together with respective discussions. Finally, some conclusions are given.

2. Experimental set-up

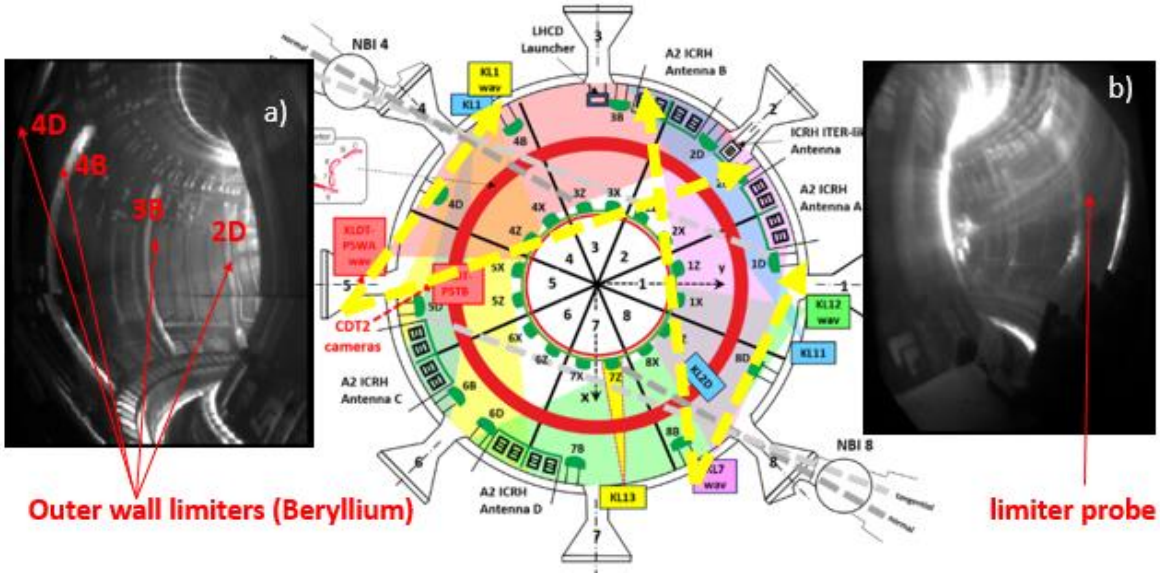

Figure 1. a) Wide-angle view of JET vacuum vessel from KLDT-E5WE during disruption. b) Equivalent view from KL8A. In the center: top schematic view of JET tokamak and viewing systems.

Both KL8A and KLDT-E5WE diagnostics are Photron APX high speed cameras with CMOS sensors (1024×1024, $20\,\mu m$ pixels) with a maximum speed of 250000 frames per second (fps) and a minimum exposure time of 1 μs for reduced Regions of Interest (ROI) of the sensor. KL8A has a remotely controllable spectroscopic filter wheel with four selectable positions. KLDT-E5WE receives the image of the JET vacuum vessel through a challenging ex-vessel set-up of beam splitters and lenses, separated from the vacuum vessel by a double fused silica window. Moreover, the light is collected from the upper and lower half of the vacuum vessel by two mirrors, forming two respective images which are combined on the camera sensor, resulting in a wide-angle view (fig. 1.a) of the JET main chamber [18].The cameras are triggered by the JET data acquisition systems and a 2GB maximum size video is stored as JET pre-processed signal. The video length depends on both the ROI size and frame rate, being from $\sim 0.5\ s$ to $\sim 10\ s$ and can be divided in separated sub-intervals. One of the most used configuration was the simultaneous observation of the outer wall region in octant 4 (KLDT-E5WE) and the divertor area in octant 8 (KL8A) (figure 2). The camera exposure times, τ_{exp}, depend on the expected light flux, which in turn depends on the plasma emission, and must be at least equal to the inverse of the frame rate. In table 1 are listed typical exposure times used for each type of observations. In table 1 are shown typical settings to observe regions of the JET vacuum vessel. Finally, the videos can be visualized and analyzed with the software JUVIL [19], specifically created to handle all the cameras of the JET viewing system. Generally, the cameras are operated without filters in order to maximize the light flux onto the sensor and thereby the frame rate. In figure 2 are shown the images of JET divertor (2.e) and outer wall (2.a) obtained with the two fast cameras, respectively. As seen in figure 2.b, the visible light at the inner divertor follows the time trace of the vertical D_α spectroscopic chords (fig 2.c) [20], indicating that the visible light at the fast camera is dominated by D_α emission.

	ELMs & Recycling Divertor	Limiters	Pellets, SPI Full view	Disruptions Full view
Frame rate (kfps)	20	20 - 10	18	18
$\tau_{exp}(\mu s)$	20 / 1 - 10	50 - 100	4 - 10 / 10 - 20	1-5
filter	D_α / no filter	No filter	No filter / NeII	No filter

Table 1. Table indicating the typical settings used in the observation of different regions of the vacuum vessel.

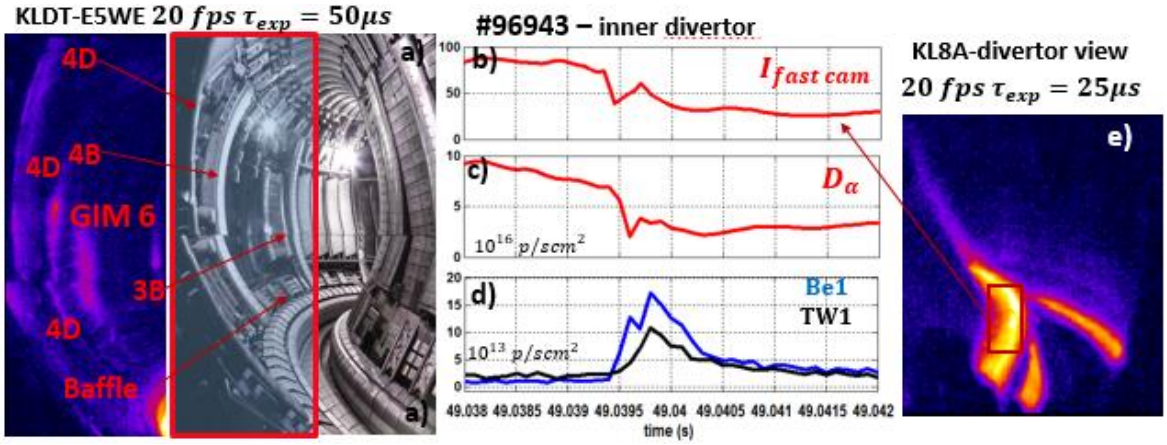

Figure 2. a) Photograph of JET vacuum vessel from KL14 endoscope and superposed image of the outer wall observed with KLDT-E5WE. In the central figure, the time trace of integrated signal from KLDT-E5WE (b) and the time trace of D_α signal measured by spectroscopy diagnostic looking to the same divertor region (c). In d) is shown the visible emission from the divertor (same instant as in a)) observed with KL8A fast camera.

3. Results and discussion:

Visible light from plasmas: The main source of visible light in the boundary region of hot fusion hydrogenic plasmas is the atomic line emission from Balmer electronic level transitions (known as D_α, $\lambda = 656.3\ nm$ in the case of Deuterium plasmas) during atomic excitation processes induced by electron collisions [17].

Observation of ELMs with fast visible cameras: During an ELM crash electrons and ions from the pedestal region loose partially their confinement and are expelled towards the wall and divertor through the separatrix by perpendicular and parallel transport, respectively [21 and there in]. A fraction of the ion fluxes, F^i, that impacts against the facing materials, penetrates into the surface and are thermalized and finally are re-emitted to the plasma as neutral atoms and molecules. This process is known as Recycling. The neutral flux, F^0, can be directly related to the impinging ion flux, F^i, through wall recycling coefficient: $F^0 = RF^i$. On the other hand, the neutral flux entering in the plasma region can be estimated by: $F^0 = K\boldsymbol{S/XB}L^{D\alpha}$. K is a geometrical factor, $L^{D\alpha}$ is the spectral radiance measured by an absolutely calibrated detector and S/XB is a coefficient which gives the number of ionization events per photon for a given atomic line [22] and is given by the Collisional-Radiative model [23]. This is only valid in ionizing conditions, i.e. when recombination can be neglected as a neutral source. This is generally valid at limiters, but not at the divertor in sufficiently low temperature-high density conditions. During the ELM crash, the level of D_α radiance measured by fast cameras clearly increases at the outer wall limiters, as seen in figures 2 and 3, indicating an increase of the ion flux towards the limiter targets. A relevant level of D_α emission is also observed at a region between limiters 4B and 3B,

labelled from now as the Gas Puff Imaging (GPI) area (fig. 2). This emission is originated at the separatrix by the plasma excitation of the puffed neutral Deuterium. In figure 3 are shown the time traces of maximum intensity at both the limiter target and the GPI area during one ELM, taken with the fast camera at 30 $kfps$ and 33μs of exposure time. The mean value of D_α emission during the discharge is higher in the GPI than in the limiter 4D, while its relative variation during the ELM event is larger at the limiter region, as seen in figure 3. The maximum peak of emission in the limiter is delayed with respect to the GPI by ~150 μ. This dynamics was repeatedly observed and its origin is still under discussion. Assuming a radial velocity of ELMs of the order of $1-5\ km/s$ [21] and a clearance in the outer wall (distance from the separatrix to the limiter) of $\sim 8\ cm$, radial velocities of up to of $1 km/s$ could be accessible with the fast camera at $> 10\ kfps$.

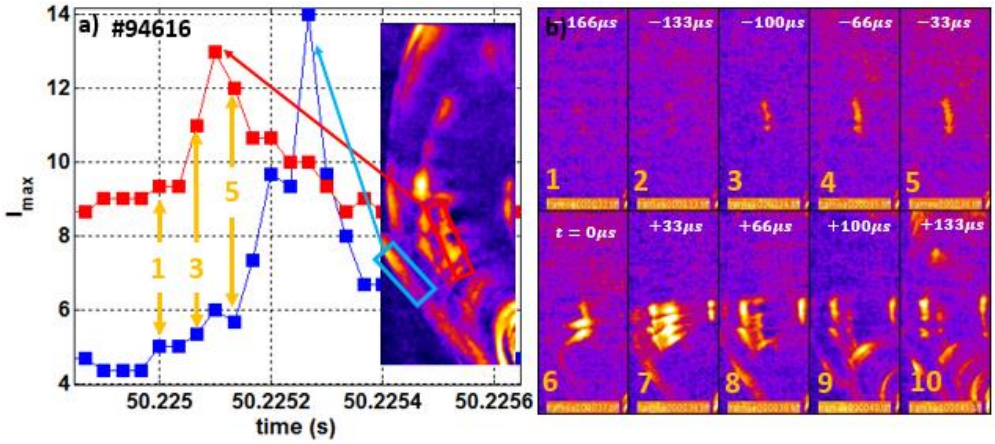

Figure 3. a) The time trace of the integrated intensity from three different ROIs at the outer wall in KLDT-E5WE. In b) is shown a set of sorted frames of de-averaged intensity during the ELM.

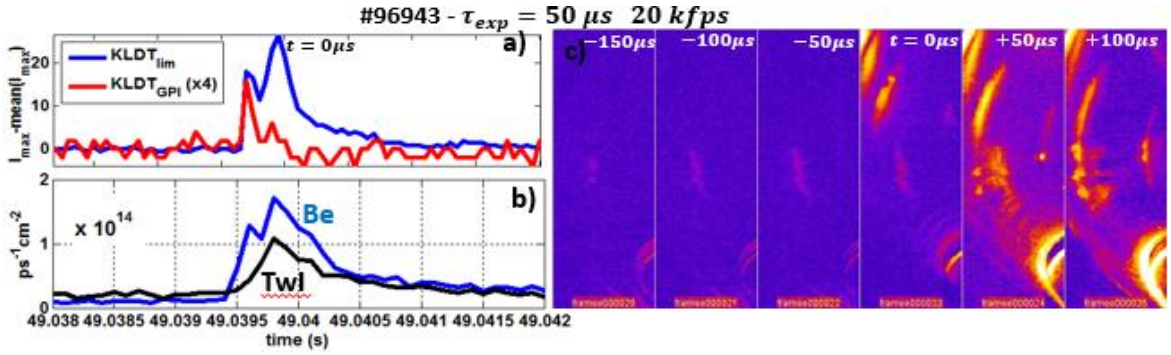

Figure 4. In a) are shown the time traces of the integrated de-averaged emission from both the outer limiter and the GPI area during one ELM. In b) are represented the time traces of Tungsten (WI: 406 nm) and Beryllium (BeII: 527 nm) from the inner divertor. c) Sorted frames at the outer wall during the same ELM.

For more intense ELMs, the described time delay is not clear (fig. 4). The reason for the sudden D_α emission in the outer limiter region is the increased ion flux, sustained during the ELM crash, with the subsequent release of recycled neutral fluxes which are then all ionized. On the other hand, the increase of the signal at the puffing is however not attributed to a change of the neutral source, which is constant, but to a modification of the edge/SOL plasma during the ELM crash that modifies the S/XB coefficient. If this is true, than the time delay of the intensity increase at the different regions can be attributed to the "time of flight" of the plasma ELM front.

Finally, the maximum D_α emission measured by the fast camera at the outer limiter 4B follows the time trace of the ion saturation current measured by a Langmuir probe installed at the midplane region of the outer limiter (figure 5). This allows the study of the filamentary character of ELMs.

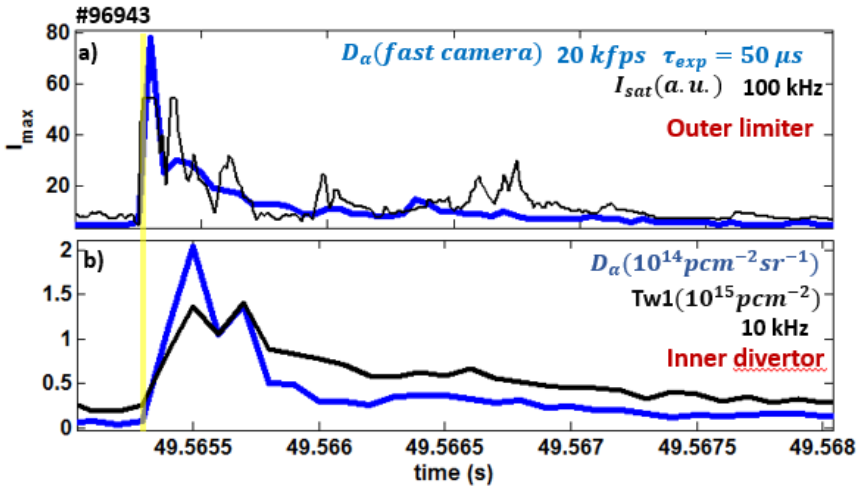

Figure 5. a). Time traces of both fast camera and limiter Langmuir probe. In b) are shown the time traces of D_α and Tungsten impurity lines measured by spectroscopic lines at the inner divertor.

Observation of Shattered Injected Pellets: Plasma disruptions lead to strong heat and electromagnetic loads against the wall. An innovative strategy is taken in order to mitigate that loads: the injection of large cryogenic pellets (SPI pellets). The pellets are composed of Deuterium, Neon or a mixture of both, and are propelled by compressed Deuterium gas towards an injection valve located at the top of JET octant 1 [24]. KL8A sensor can collect the D_α produced by the Deuterium pellet when it penetrates into the plasma and is ablated as well as the propellant gas at the top of JET octant 1. The high speed (up to 18 kHz with full sensor) allows the observation of the pellet trajectory inside vacuum chamber. Simultaneously, KLDT-E5WE observes the plasma breakdown at octant 4. In the case of Neon pellet, the filter wheel allows the observation of Ne I atomic line (visible at 692,8 nm). Figure 6 shows a SPI 100% Neon pellet entering into the plasma and recorded with a 50 μs exposure time.

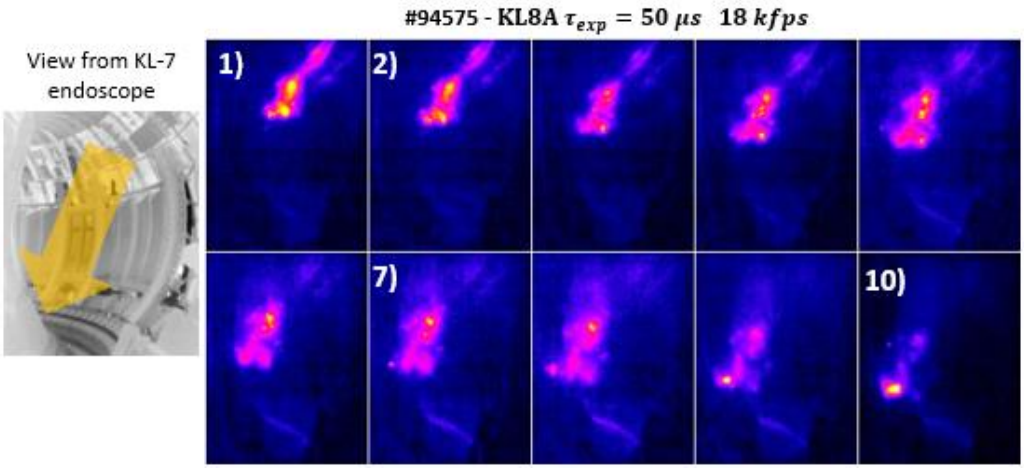

Figure 6. a) Penetration of SPI large pellet into the plasma during a disruption. Each frame is an average over 7 frames in order to don't show 70 frames. In frame 1) we see the propellant gas entering the vacuum chamber. In frame 7) some parts of the pellet impact the inner wall. In frame 10) the pellet mostly impact the inner wall.

4. Conclusions:

In the present work we have described the two fast visible cameras operating in JET-ILW. We have also shown recent observations made by fast cameras during the last experimental campaign: The use of fast cameras allows the simultaneous observation of a large fraction of the whole tokamak vessel with the adequate settings. The radial propagation of ELMs towards the outer limiters could be resolved with recording speed $> 10\ kfps$ and with exposure times $\tau_{exp} > 33\ \mu s$. Studies on turbulence in the Scrape-off layer are possible during ELM phases by observing the fluctuations in D_α emission with KLDT fast camera at speed $> 10\ kfps$. In addition, the simultaneous use of the two fast imaging systems is crucial in the observation of SPI pellets and their effects. In addition, fast imaging has demonstrated its utility in the study of other topics, not treated here, such as: disruptions, pacing pellets, divertor recycling dynamics, study of of L-mode and ELM filaments, among others.

Acknowledgements: This work has been carried out within the framework of theEURO fusion Consortium and has received funding from the Euratom research and training programme 2014–2018 undergrant agreement No. 633053. The views and opinions expressed herein do not necessarily reflect those of the Eur-opean Commission.

References:

[1] F. Romanelli on behalf of JET Contributors (2015) Nucl. Fusion 55 104001
[2] X. Litaudon et al. (2017) Nucl. Fusion **57** 102001
[3] G. Arnoux et al. (2012) Rev. Sci. Instrum **83(10)** 10D727
[4] A. Huber *et al* (2018) *Nucl. Fusion* **58** 106021
[5] I. Balboa et al. (2012) *Review of Scientific Instruments* **83**, 10D530
[6] S. Salasca et al., (2009) Fusion Engineering and Design **84** 7-11 pp 1689-1696
[7] J. W. Ahn et al. (2010) Review of Scientific Instruments **81**, 023501
[8] N. Nishino *et al 21st IEEE/NPS Symposium on Fusion Engineering SOFE 05*, Knoxville, TN, (2005), pp. 1-6, doi: 10.1109/FUSION.2005.252963
[9] J. H. Yu et al., (2009) Journal of Nuclear Materials **390-391** pp 216-219
[10] A. L. Roquemore *et al*., (2007) *IEEE 22nd Symposium on Fusion Engineering*, Albuquerque, NM, pp.1-4
[11] A Kirk *et al* 2016 *Plasma Phys. Control. Fusion* **58** 085008
[12] E. de la Cal et al., Contrib. Plasma Phys. (2010) **51**, No. 8, 742 – 753
[13] S. B. Ballinger et al. (2018) Nuclear Materials and Energy **17** pp 269-273
[14] A. Alonso et al. (2008) AIP Conference Proceedings **988** 185
[15] E. Gauthier et al. (2007) Fusion Engineering and Design **82** 5-14 pp. 1335-1340
[16] C. Reux *et al* (2015) *Nucl. Fusion* **55** 093013
[17] T. Fujimoto, (2008) Plasma Spectroscopy. Springer Berlin Heidelberg, Berlin, Heidelberg
[18] M. Clever et al. (2013) *Fusion Engineering and Design* 88 1342– 1346
[19] V. Huber et al. (2017) *Fusion Engineering and Design* **123** pp 979-985
[20] E de la Cal *et al* (2020) *Plasma Phys. Control. Fusion* **62** 035006
[21] C Silva *et al* (2009) *Plasma Phys. Control. Fusion* **51** 105001
[22] K H Behringer et al, (1987) J. Nucl. Mater. 145-147
[23] L. C. Johnson. (1972) The Astrophysical Journal, 174:227
[24] S. J. Meitner et al., Fus. Sci. Tech. 72 (2017) 318